JOURNAL OF Applied Polymer SCIENCE

Silibinin Binding and Release Activities Moderated by Interstices of Trimesoyl, Tridimethyl, and Tridiethyl Malonate First-Tier Dendrimers

Sachin B. Undre,[1] Man Singh,[1] R. K. Kale,[1,2] Md. Rizwan[3]

[1]School of Chemical Sciences, Central University of Gujarat, Gandhinagar 382030, India
[2]School of Life Sciences, Jawaharlal Nehru University, New Delhi 110067, India
[3]Centre for Nano Sciences, Central University of Gujarat, Gandhinagar 382030, India
Correspondence to: M. Singh (E-mail: mansingh50@hotmail.com)

ABSTRACT: Trimesoyl 1,3,5-tridimethyl malonate (TTDMM), trimesoyl 1,3,5-tridiethyl malonate (TTDEM), trimesoyl 1,3,5-tridipropyl malonate, trimesoyl 1,3,5-tridibutyl malonate, and trimesoyl 1,3,5-tridihexyl malonate first-generation dendrimers, a complete series of dialkyl malonate esters from methyl to hexyl, were synthesized by a divergent growth approach with about a 95% yield. TTDMM and TTDEM members of this series were characterized with 500-MHz NMR and Fourier transform infrared spectroscopy. The 7.469353 and 8.435395 m^2/g surface areas and 700.1907- and 792.6436-nm pore-average diameters of TTDMM and TTDEM, respectively, implied that they could be used as prospective drug binders. Alkyl chains from methyl to hexyl of dialkyl malonate esters had enhanced interstitial spaces to trap the drugs and toxic heavy metals for their distribution and bioremediation, respectively. Thus, the dendrimers, silibinin (SB) complexes in a 1:1 ratio with acetone, were prepared and studied with Fourier transform infrared spectroscopy, differential scanning calorimetry, dynamic light scattering, scanning electron microcopy, and atomic force microscopy. The ultraviolet–visible spectroscopy at a 330-nm lamda max (λ_{max}) showed about 5%/h SB released in phosphate buffered saline with 10% dimethyl sulfoxide. The objective was used to investigate the capacity of dialkyl malonate terminated dendrimers to encapsulate a maximum amount of SB and anticancer drugs and the *in vitro* releasing activity. © 2013 Wiley Periodicals, Inc. J. Appl. Polym. Sci. 130: 3537–3554, 2013

KEYWORDS: biocompatibility; biomaterials; dendrimers drug-delivery systems; hyperbranched polymers and macrocycles; molecular recognition

Received 20 January 2013; accepted 23 April 2013; Published online 26 June 2013
DOI: 10.1002/app.39466

INTRODUCTION

The synthesis of architectural dendrimers by potential molecules is being considered as a new area for multitasking materials with better activities to catalyze chemical and biochemical processes. Thereby, in the early 1970s, a synthesis and characterization of dendrimers was initiated by Vogtle.[1] Also in 1984, a first family of macromolecules hyperbranched like a starburst was developed by Tomalia et al.,[2] and others also have focused on their synthetic methodologies and applications.[3,4] Thus, a critical transition for supramolecular structures is seen as a new trend for the development of multiapplications of a single molecule.[5,6] In general, their synthesis has been made either through convergent or divergent approaches.[7–9] For a long time, composites of several molecular species with required physicochemical properties have been prepared.[10,11] Protein, starch, and DNA as giant molecules are naturally occurring, but their embedded functional groups are not able to interact with drugs or other similar molecules and cannot be used as drug vehicles. Thereby, their activities are to be designed and catalyzed by molecular interactions materialized through cohesive forces and intermolecular forces (IMFs).[12,13] Thus, the dendrimer could play a critical role in entering the embedded structures of giant molecules through their tentacles to alter their structural activities. However, the proteins have been shown to be entropy driven because of the weakening of peptide polar bonds, whereas the dendrimers initiate tentropy- and enthalpy-driven activities in biochemical processes because of the oscillations of their tentacles when they enter networks of hydrogen bonds. Thereby, a series of dialkyl malonate esters as branching units with trimesoyl chloride (TMC) have been developed for interacting activities with silibinin (SB) for the development of encapsulation for better transportation. Several scientists have used molecules such as melamine as a core for the synthesis of dendrimers,[5–9] but the TMC, with three binding sites, is now considered as a potential core with a special significance for binding branching molecules. Also, so far, no scientist has used a series of dialkyl malonate esters to act as branchings of the dendrimers with varied entropies caused by oscillations caused by elongation of the alkyl chains. This has led to the synthesis

of divergent dendrimers with TMC as a core at center with a single tier of dimethyl to hexyl malonate esters as branching units with the pattern of Tomalia et al.[8,14] The methyl and hexyl groups remain at the terminal position and oscillate freely as tentacles to attain an equilibrium that initiates entropy and entropy out of intermolecular multiple force theory (IMMFT).[10] To the best of our knowledge after an intensive literature survey, trimesoyl 1,3,5-tridimethyl malonate (TTDMM), trimesoyl 1,3,5-tridiethyl malonate (TTDEM), trimesoyl 1,3,5-tridipropyl malonate (TTDPM), trimesoyl 1,3,5-tridibutyl malonate (TTDBM), and trimesoyl 1,3,5-tridihexyl malonate (TTDHM), the first generation (G_1) dendrimers, have never been synthesized before, but now they may be proven helpful for drug design and release systems and for trapping oxygen for masking CO_2 and CO gases from an air sample. These dendrimers could be used as gas-sorting and heavy-metal-trapping sensors. The O_2 could be trapped in the void spaces caused by their optimized geometry with better catalytic activities and could lead to the development of acoustic blends due to their branching. This relationship could be fascinating from a nanotechnology point of view with the elongation of dialkyl chain of esters having innumerable interstices; this leads to a concept of acoustivity, and these could be most suitable materials for the aggregation of nanoparticles on a pattern of alkane thiols. The latter has never been cited in dendrimers except as an interstitial networking in context of the bioremediation of Hg, Cd, Pb, and other toxic heavy metals. The dendrimers themselves, on getting trapped with the transitional and lanthanide metals, could act as piezoelectric materials or effective biomaterials; this could be extended to SiO_2, TiO_2, Al_2O_3, and Fe_2O_3 nanoparticles and many others in the form of molecular self-assembly. Such materials may be useful for coding, decoding, moisture, heat, volume, and potential sensors and to retrieve information about defense applications. NMR, Fourier transform infrared (FTIR) spectroscopy, differential scanning calorimetry (DSC), and their surface areas have implied the possibilities of such applications. The formulation of highly efficient drug-binding materials has been a centuries-old challenging task for better and safer curing of the disease because effective curing depends on efficient drug delivery. The binding of a drug in a most wanted manner, transport to target sites, and release in a desired manner has been a great concern to pharmacists.[15–19] To avoid structural exchange during a whole process, the encapsulation, cavity, and capping with nonionic surfactants such as sorbitol, tweens, guar gums, and agar need critical models to perform this role in a most optimum manner. Thus, dendrimers have been found to be befitting entities, although the uneven distribution of their electrostatic charges has been a slight restriction that could damage the drug structure and efficiency because of the possibility of chemical reactions. Therefore, the dendrimers as vehicles must not react or damage drug structures during the binding and carrying processes. Singh et al.[6,11] reported 2,4,6-tridiethyl malonate triazine (TDEMTA), 2,4,6-hexadiethyl malonate triazine (HDEMTA), 1,3,5-triglycerate-triazine, and tri(1,3,5-triglycerate) triazine dendrimers with certain safer binding molecules, such as poly(vinyl pyrrolidone), glycerol, and sodium diethyl malonate esters (SDEME). With this pattern, TTDMM and TTDEM have been characterized and used to bind SB and release. The dendrimers have discrete activation energies against the law of mass actions because they very quickly get equally distributed with their similar size without causing size-based energy gradients in their particles, as depicted with dynamic light scattering (DLS). There is a controlled energy distribution in tiers with excellent IMMFT because they have almost equal networking centers within their structures. The isotropic and anisotropic changes of TTDMM and TTDEM structurally influence the binding and release of SB from the vehicle.

EXPERIMENTAL

Materials

Trimesoyl chloride, sodium metal, dimethyl, diethyl, dipropyl, dibutyl, and dihexyl malonate esters; methanol (MeOH); SB; acetone (Sigma-Aldrich); dimethyl sulfoxide (DMSO; Rankem India); and ethanol (EtOH; Scvuksmandli, Ltd.) were used as received and were stored overnight in a vacuum desiccator filled with P_2O_5 until use. The moisture was checked with anhydrous $CuSO_4$.

Drug–Dendrimer Complexes: Preparation and Characterization

SB–TTDMM and SB–TTDEM complexes were prepared at 1:1 mol/mol in 20 mL of acetone with constant stirring at 400 rpm for 12 h at room temperature (RT). After 15 min, the acetone was evaporated at 56°C *in vacuo* with a rotary evaporator (Rotavapor R-210, Buchi, Switzerland). ^{1}H-NMR was recorded with a Bruker 500-MHz Ultrashield Plus instrument with $CDCl_3$ (E-Merck, 99.9%) as a solvent and TMS as an internal reference. The FTIR spectra for TTDMM, TTDEM, SB, SB–TTDMM, and SB–TTDEM were recorded with a PerkinElmer 65 series FTIR spectrophotometer with 1.5–2.0-mg samples in a pelletized form with KBr. DSC analysis was done with a DSC 6000 PerkinElmer instrument from 50 to 250°C at a 10°C/min heating rate, and 2-mg samples were packed in aluminum pellets. The surface area and pore size were measured with a Thermo Scientific surfer gas adsorption porosimeter with the Brunauer–Emmett–Teller (BET) method.[20] The pore structure was elucidated with the Barrett, Joyner, and Halenda (BJH) method.[21] The 0.4-g sample was degassed in a sample tube at 100°C for 3 h under a 9×10^{-4} Torr vacuum and was placed in liquid nitrogen. The mean diameter (MD) and polydispersity index (PDI) was determined with DLS (Microtrac Zetatrac Metrohome). Amounts of 0.2 mg of TTDMM, TTDEM, and SB were separately dissolved in 10 mL of Tween 60 to determine the particle size. Amounts of 0.2 mg of the SB–TTDMM and SB–TTDEM complexes were separately dissolved in 10 mL of Tween 60 as a dispersant medium for DLS (Table III, shown later). The surface morphology of the dendrimers and complexes were studied with scanning electron microscopy (SEM; Carl Zeiss, EVO-18, operated at 20 kV). The solid sample was coated with a thin layer of palladium and gold in 80:20 ratios by sputtering at a 5-μA current up to 60 s. Topographical studies of the dendrimers and drug–dendrimer complexes prepared in chloroform with atomic force microscopy (AFM; XE-76 advanced scanning probe, Park System Corp.) were done in noncontact mode under a set phase and amplitude. A small volume of the each dendrimers and complex solutions were placed on a 10×2.5-cm^2 glass slide and imaged after drying in air. The silicon cantilever was in noncontact tapping mode.

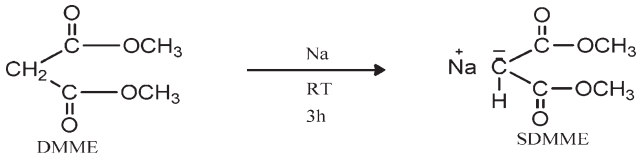

Scheme 1. Synthesis of SDMME.

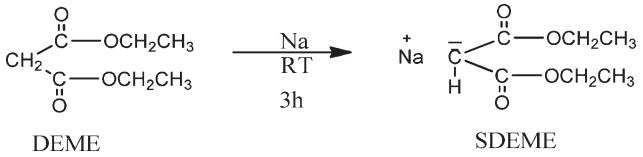

Scheme 2. Synthesis of SDEME.

In Vitro Drug-Release Analysis

Concentrations of 25, 50, 75, 100, and 125 μM SB were dissolved in phosphate buffered saline (PBS) plus 10% DMSO (PD) for the calibration curve. The 10-mg complex was dissolved in 100 mL of PD and stirred continuously at 500 rpm at 37°C in a 100-mL beaker. From 0 to 10 h, the 2.5-mL sample was taken with a 0.20-μm sterile syringe filter (Corning, Germany) for UV analysis. The SB release was determined with UV absorbances at 245, 285, and 330 nm with an ultraviolet–visible (UV–vis) spectrophotometer (Analytical Technologies) and calculated with eqs. (1) and (2):[22–25]

$$A = \epsilon \times l \times c \tag{1}$$

where A is the absorbance, ε is the molar absorptivity, l is the cell path length (cm), and c is the SB composition with 0.000125 mM. A was 2.187, and l was 1 cm. With these values placed into eq. (1), ε = 17496 m^2/mmol was found at lamda max (λ_{max}) = 330 nm:

$$Drug\ release\ (\%) = \frac{SB\ released}{Amount\ of\ SB\ in\ the\ substrate} \tag{2}$$

RESULTS AND DISCUSSION

Synthesis

Sodium metal and dimethyl malonate esters (DMMEs) in a 1:1 ratio were placed in a 50-mL round bottom (RB) flask and were stirred at RT. After 3 h, a white, solid sodium dimethyl malonate ester (SDMME) was obtained (Scheme 1), where the reaction was slightly exothermic at temperatures from 25 to 44°C. Similarly, for SDEME synthesis, dimethyl malonate ester (DMME) was replaced by diethyl malonate ester (DEME) in similar stoichiometric ratios within similar experimental conditions (Scheme 2). Then, after 3 h, a white, solid product was formed. The DEME reaction was exothermic; this raised the temperature from 25 to 45°C. A temperature difference of 1°C in both the reactions was found because of —CH_2 activities in the case of DEME. TMC and SDMME were placed in a 50-mL RB flask at a 1:3 ratio in MeOH stirred constantly for 3 h at

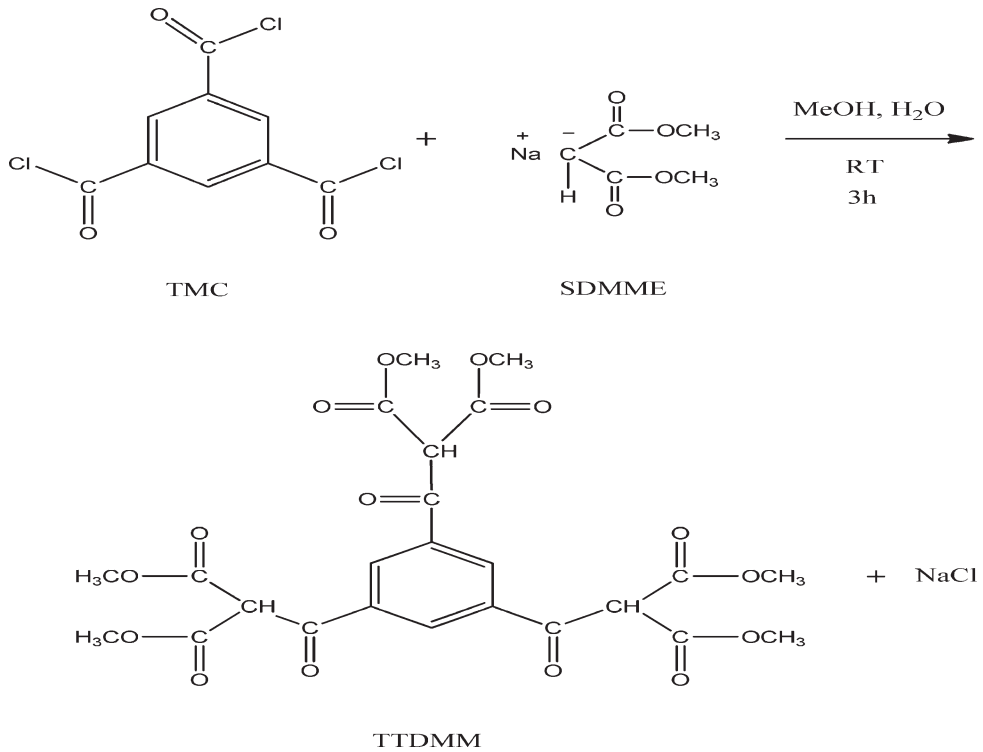

Scheme 3. Synthesis of TTDEM.

RT. The temperatures from 25 to 62°C could have been due to the dissociation of two ionic bonds, out of which one of the bonds came from TMC and another came from SDMME (Scheme 3). On the formation of NaCl, the energy might have been released; this led to a higher temperature. The NaCl with less affinity in the mixture was settled at the bottom. The products were filtered through a Whatmann filter paper no. 42. The NaCl was removed with almost five washes with ice-cold water, and its presence was checked by the testing of the filtrate with aqueous $AgNO_3$ as follows:

$$AgNO_3\,(\text{aqueous}) + NaCl\,(\text{aqueous}) \rightarrow AgCl\,(\text{white precipitate}) + NaNO_3\,(\text{aqueous}) \quad (3)$$

The final product was dried in a vacuum oven for 3 h and stored in a P_2O_5-filled desiccator at normal temperature pressure (NTP), and the yield was 95% (Scheme 3). TTDEM was synthesized in a similar manner, except with SDEME in place of SDMME (Scheme 4). The reaction was exothermic; this increased the temperature from 25 to 64°C for TTDMM synthesis with a 95% yield. A difference in the temperature by 2°C implied an impact of the —CH_2 with a higher heat content. TTDPM, TTDBM, and TTDHM were prepared by placing TMC with dipropyl, dibutyl, and dihexyl individually at 1:3 ratios (Scheme 5). The reactions were analyzed with thin-layer chromatography on aluminum-based silica gel plates. The dendrimers with longer alkyl chains showed larger surface areas, and the study of their physicochemical properties studied with survismeter and applications in the binding and release of SB and mathotrexate, anticancer drugs, are being pursued in the laboratory and should be communicated in a future article. The structure of TTDHM, a higher member of the series, is shown in the following structure:

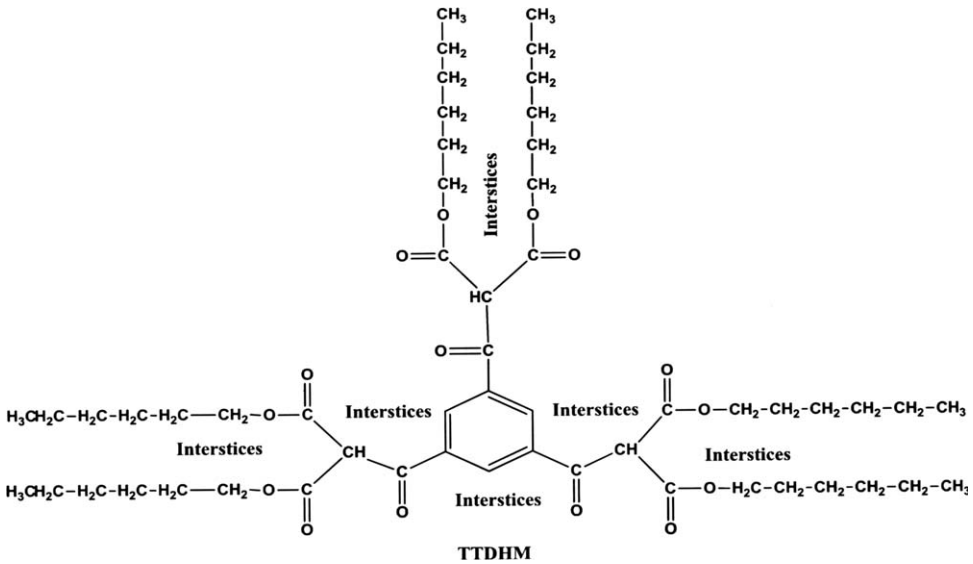

^{1}H-NMR for Structure Elucidation

NMR elucidated the states of ^{1}H and ^{13}C because of the shielding and deshielding effects that made TMC produce a sharp peak at 9.116 ppm for Ar—H and at 7.287 ppm for the C_6 $CDCl_3$ [Figure 1(a)]. The value at 9.1116 ppm depicted a core structure and peaks of —CH_2 and —OCH_3 at 3.326 and 3.670 ppm, respectively, with DMME [Figure 1(b)]. We observed a singlet of —CH_2 at 3.347, a quartet of —CH_2 at 4.211, and a triplet of —CH_3 at 1.280 in DEME [Figure 1(c)]. The ^{1}H-NMR for TTDMM and for —CH— of ester showed a singlet at 2.146 ppm and for —OCH_3 showed a singlet at 3.954 ppm; the peak for C_6 $CDCl_3$ remained at 7.239 ppm [Figure 1(d)]. The Ar—H was at 8.830 ppm with a minor change compared to the TTDEM from 9.116 to 8.830 ppm with a net variation of 0.286 ppm for TTDMM and was applicable for TTDEM structural analysis [Figure 1(e)]. A singlet at 2.200 ppm for —CH was present in both dendrimers. A quartet from 1.277 to 1.464 ppm for —CH_2 and a triplet peak from 4.318 to 4.611 for —CH_3 with —CH_2 of ester groups were observed [Figure 1(e)]. The 8.877-ppm peak implied Ar—H and —CH protons of esters at 2.146–2.200 ppm with a 0.054-ppm difference. Thus, weak, steric, and induction effects of —CH_2CH_3 and the electronegativity of >CO destabilized —CH comparatively at lower fields. Steric and induction effects with TTDMM were noted due to >CO in both the sides and were weakly deshield; then, a peak was seen at a higher field. Thus, alkyl chain of esters influenced the spectroscopic behavior of the —CH— proton. Although the —CH— protons must have fallen at high fields, with TTDMM, it fell at 3.954 ppm, a lower field. The protons of —CH_3 due to a higher electron density at the O atom led to a spinning of the —CH_3 proton at lower field. With TTDEM, the —CH_3 appeared from 1.277 to 1.464 ppm, a high field, in a closely pack quartet. The TTDEM with terminal —CH_3 should have given a single peak, but the —CH_3 was attached to an oxygen, a highly electronegative atom, with a coupling constant that showed a closely packed quartet [Figure 1(e)].

FTIR Spectroscopy for the Stretching of the Dendrimers in Complexes

FTIR spectroscopy depicted the stretching frequencies of ester, >CO, and similar others, where the 1004-cm^{-1} stretching frequency depicted the stretching of C—H in-plane bending and

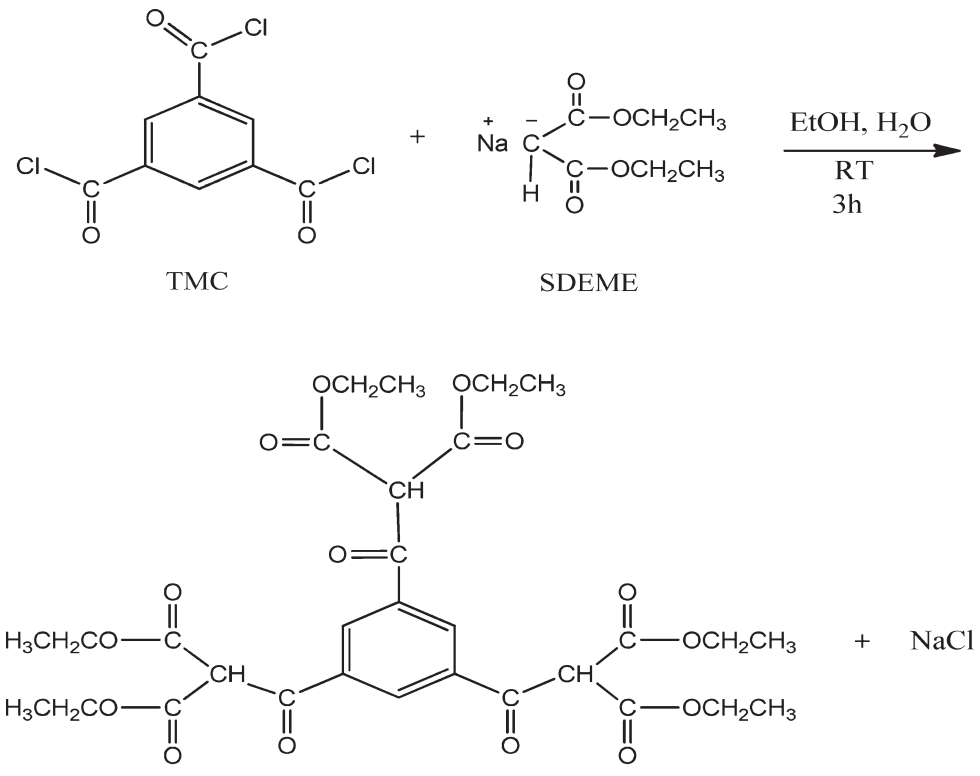

Scheme 4. Synthesis of TTDEM.

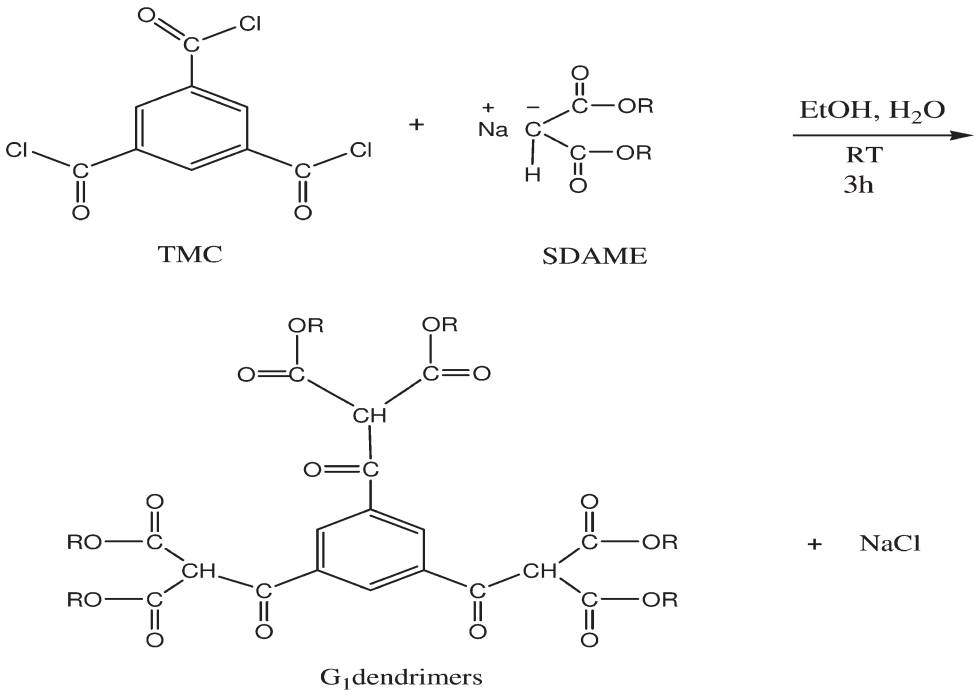

R = $-CH_2CH_2CH_3$, $-CH_2CH_2CH_2CH_3$, $-CH_2CH_2CH_2CH_2CH_2CH_3$

SDAME = Sodium dialky malonate esters

Scheme 5. Synthesis of TTDPM, TTDBM and TTDHM.

Applied Polymer SCIENCE

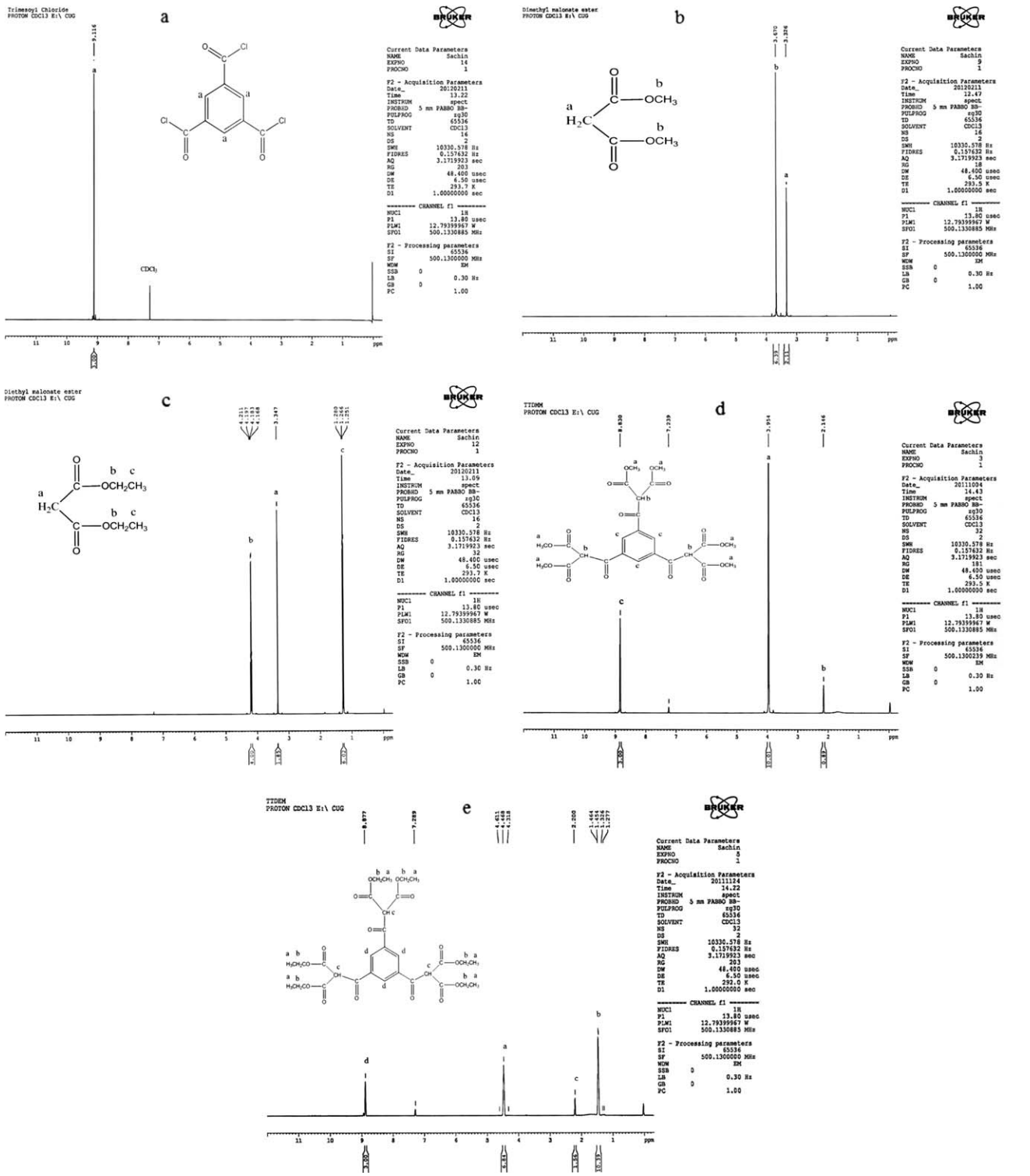

Figure 1. ^{1}H-NMR spectra of (a) TMC, (b) DMME, (c) DEME, (d) TTDMM, and (e) TTDEM.

stretching at 739.68 cm^{-1} for out-of-plane bending in TTDMM [Figure 2(a)]. The 1431.8–1455-cm^{-1} band indicated aromatic C═C bonds (core), and the bands from 930.3 to 1253 cm^{-1} denoted C—O bending stretching. The aromatic ring and >CO of the malonate esters were at 1618.4 and 1735 cm^{-1}, respectively, and the band at 1342.4 cm^{-1} implied the C—O stretching of the malonate esters. The 3018.2- and 3092-cm^{-1} band showed C—H stretching of an aromatic ring, and the 2851-cm^{-1} band depicted sp^3 C—H stretching. The C—H stretching of the O—CH_3 at the terminus appeared at 2956 cm^{-1}, and an

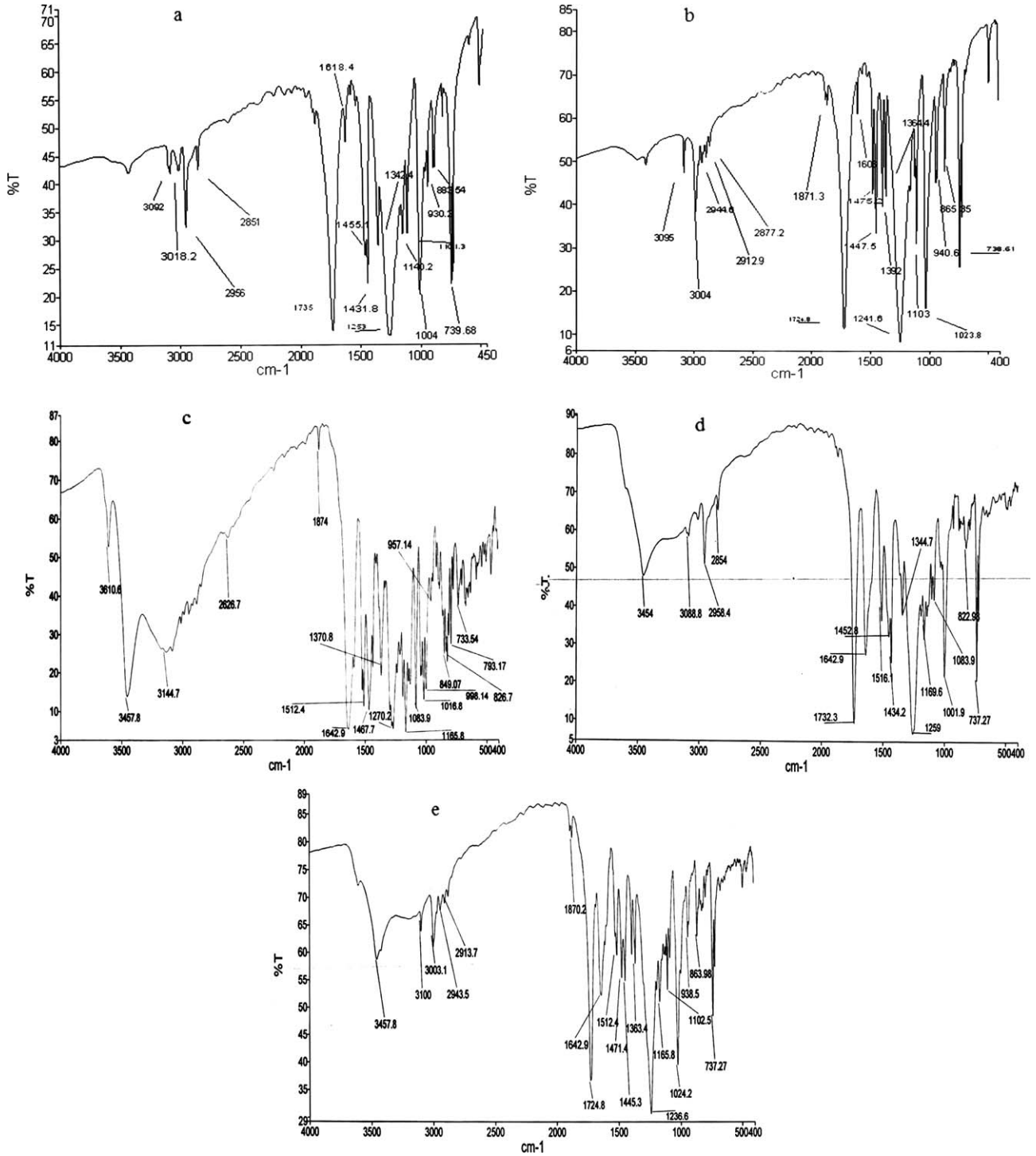

Figure 2. FTIR scans of (a) TTDMM, (b) TTDEM, (c) SB, (d) SB–TTDMM, and (e) SB–TTDEM.

extra band at 2993.9 cm^{-1} appeared for —C—H— was observed and attached at a terminal —CH_3 of ester in TTDEM [Figure 2(b)] against TTDMM [Figure 2(a)]. In TTDEM, C—H bending appeared at 1025 cm^{-1} for in-plane bending and at 736.78 cm^{-1} out-of-plane bending, and aromatic C=C stretching appeared at 1447 cm^{-1}. The aromatic ring and >CO of ester appeared at 1606.1 and 1728.6 cm^{-1}, respectively. The C—H stretching of the aromatic ring appeared at 2956 cm^{-1}, and the band at 2851 cm^{-1} depicted sp^3 C—H stretching; the same stretching was noted with TTDMM. The C—O stretching frequency for ester appeared at 1350 cm^{-1}, and the C—H stretching band of terminal O—CH_2—CH_3 appeared at 2940.8 cm^{-1} [Figure 2(b)]. The SB, with —OH, may have formed a complex with ester groups, where the FTIR stretching frequencies for —OH with SB, SB–TTDMM, and SB–TTDEM were at 3457.8, 3454, and 3457.8 cm^{-1} with 15, 50, and 60% transmissions, respectively [Figure 2(c–e)]. A

Applied Polymer SCIENCE

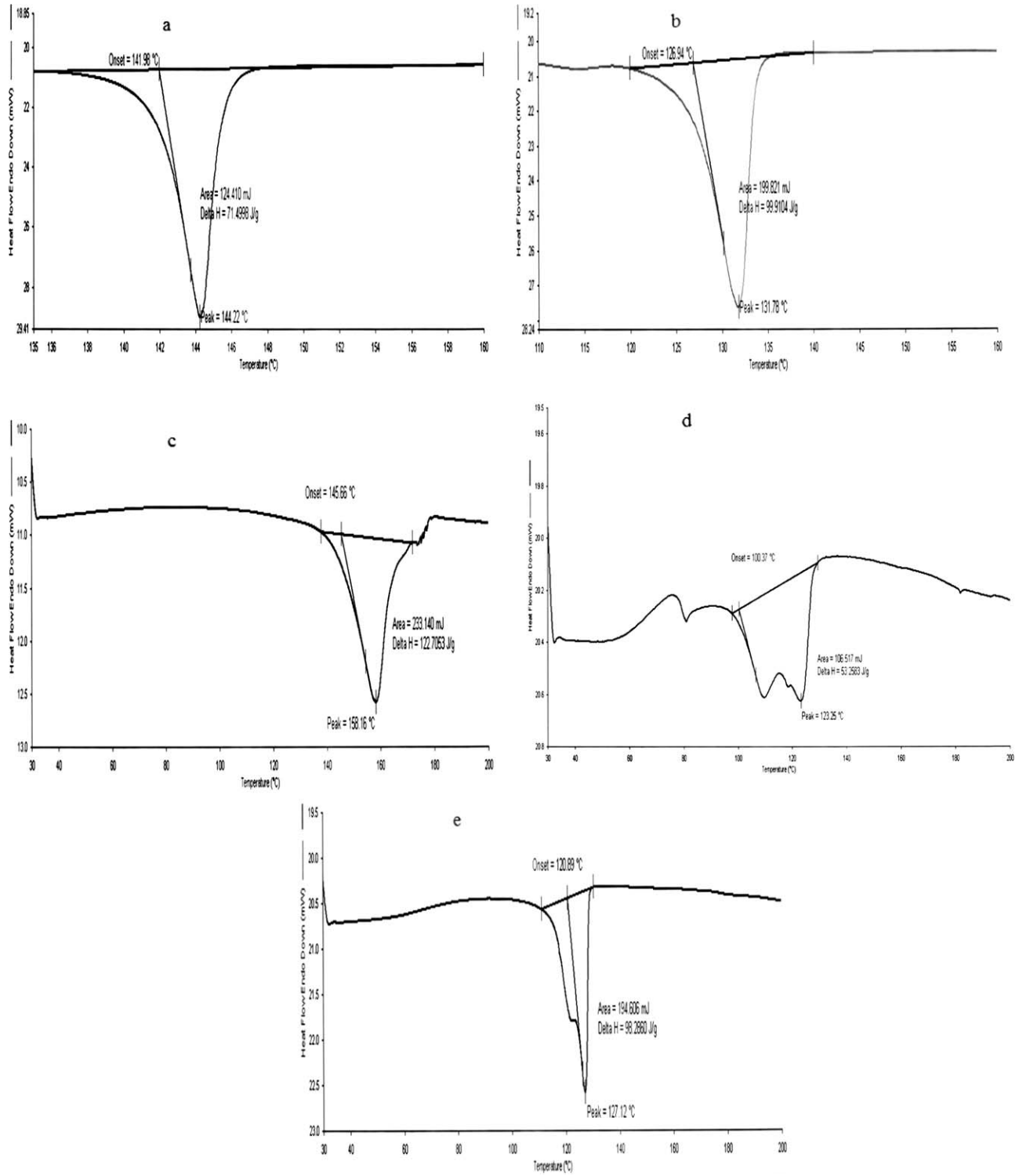

Figure 3. DSC thermograms (a) TTDMM, (b) TTDEM, (c) SB, (d) SB–TTDMM, and (e) SB–TTDEM.

stretching frequency for —OH, which was missing in TTDMM and TTDEM [Figure 2(a,b)], confirmed that the SB formed complexes with them. >C═O absorbances with SB, TTDMM, and TTDEM were observed at 1642.9, 1735, and 1724.8 cm^{-1}, respectively. The >C═O absorbance peak at 1724.8 cm^{-1} with SB–TTDEM, in the same region, was observed with TTDEM.

The >C═O peak shifted from 1735 to 1732.3 cm^{-1} with SB–TTDMM as compared to the TTDMM. The pure SB showed a stronger carbonyl band absorbance at 1642.9 cm^{-1} of the ring ketonic group in SB. Also, this band was noted in both the complexes at the same region but was missing with TTDMM and TTDEM. The peaks from 1200 to 1000 cm^{-1} indicated the

benzene ring as the core in TTDMM and TTDEM [Figure 2(a,b)]. With both complexes, these peaks were found in the same region [Figure 2(d,e)]. The peaks at 2851 and 2877.2 cm^{-1} denoted the C—H stretching vibration of the C—H bond in malonate ester groups of the dendrimers. The C—H stretching vibration shifted slightly from 2851 to 2854 cm^{-1} with SB–TTDMM and from 2877.2 to 2874 cm^{-1} with SB–TTDEM. The 1618.4- and 1608-cm^{-1} bands implied C=C stretching of the core and shifted from 1618 to 1516.1 cm^{-1} and from 1608 to 1512.4 cm^{-1} with SB–TTDMM and SB–TTDEM, respectively [Figure 2(d,e)]. FTIR spectroscopy implied a surface functionality in them that played a critical role in the complexation with the SB.

DSC of the Dendrimers in the Complexes

DSC indicated a phase transition as a function of IMF in terms of the onset temperature and enthalpy due to a transition of the dendrimers. A single-endotherm thermogram in TTDMM and TTDEM implied a phase transition. DSC of TTDMM and TTDEM showed major endotherms at 141.98 and 126.94°C, respectively; these were attributed to an onset of MP with the formation of a phase [Figure 3(a,b)]. The 144.22 and 131.78°C MPs were found to be TTDMM > TTDEM [Figure 3(a,b)] and were higher by 12.44°C because of —CH_2 in TTDEM as compared to TTDMM with a weaker IMF with TTDEM. The —CH_2 induced hydrophobic interactions with stronger covalent forces and an induction effect, a factor for interaction with the electron-releasing capacity of terminal —CH_3 in TTDEM. An electron releasing capacity of —CH_3 might have not been disrupted by —CH_2, which was missing an extra sp^3 configuration and could have formed carbon nanotubes because of the polymerization of carbon atoms on a pattern of graphene.[26] In dendrimers, the core, >CO, and ester groups are common. Because oxygen atoms are electronegative in nature and —CH_3 is electron-releasing, —CH_2 of TTDEM may offer modeling of IMF, which could develop applications of Columbic forces of attraction.[27] The —CH_3 electron-releasing capacity is disrupted by —CH_2; this resulted in a lower MP of TTDEM [Figure 3(a,b)]. The electron-releasing strength of —CH_3 was executed via an induction effect caused by —CH_2; this could have caused piezoelectric and acoustic properties. The change in enthalpy (ΔH) data focused their heat-holding capacities for a transition because enthalpy is conserved in chemical bonds and a higher ΔH is fitted with a relationship between the energy and number of carbon atoms. TTDMM had one carbon atom at a terminal, and TTDEM had two atoms; the ΔH relationship was as TTDEM > TTDMM, and the surface area relationship was TTDEM > TTDMM.

The distribution of ΔH in the TTDEM area was larger than that in TTDMM. The onset temperature of TTDMM was 141.98°C because a higher energy was required to weaken the IMFs for its melting; the TTDEM onset temperature was 126.94°C [Figure 3(a,b)]. These data implied that the TTDEM comparatively developed weaker IMFs at NTP because of a distribution of ΔH. Their melting was attained in a comparatively shorter time and at a lower temperature because TTDEM was larger than TTDMM and the flow or distribution of ΔH was larger in area than TTDMM. The —CH_3 of the TTDEM has shown the similarities in behavior and is also proven with chemical shift in NMR [Figure 1(a,b)]. Compared to the TTDMM, variations in the ΔH, area, onset, FTIR spectroscopy, NMR, and surface area of TTDEM proved to have effects on the —CH_2 activities. The DSC spectra showed only one broad endotherm for complexes compared to the endotherms of TTDMM, TTDEM, and SB [Figure 3(a–c)]. The onset temperatures for SB, SB–TTDEM, and SB–TTDMM were 145.66, 120.89, and 100.37°C, respectively [Figure 3(c–e)]. Here, the SB and dendrimers had their own structures in complexes with different heat capacities; this produced two different peaks in the DSC spectra [Figure 3(d,e)], and the diffusion of a broad band confirmed complex formation. A variation in ΔH with complexes implied structural intermixing for the development of a single phase with the least entropy. The onset temperature relationship was TTDEM > TTDMM, and the DSC of TTDEM showed higher values of onset a 120°C with stronger interacting and binding activities with SB as compared to TTDMM. The SB showed higher values of onset and ΔH because of a higher capacity for complexation [Figure 3(c–e)]. The ΔH for SB–TTDEM was greater than that of SB–TTDMM (98.29 and 53.26 J/g, respectively); this showed a higher heat-holding capacity for SB–TTDEM than for SB–TTDMM. These effects were caused by the alkyl chains in TTDEM having a ΔH of TTDEM that was greater than that of TTDMM [Figure 3(a–e)]. This gave us a clear understanding of the interacting and binding activities with variable alkyl chains.

Surface Area and Pore Size

The BET method was used to determine the surface area and pore size distribution with surface areas with that of TTDEM greater than that of TTDMM [8.435395 and 7.469353 m^2/g, respectively; Table I and Figure 4(a–d)] with a higher value of TTDEM of 0.966042 m^2/g. This reflected a contribution of each —CH_2 of 0.161007 m^2/g (Table I). Hence, dendrimers with an increase in alkyl chains showed a higher surface area and could

Table I. Surface Areas (m^2/g) and Pore Size Distributions (nm) of TTDMM and TTDEM

Calculation method	TTDMM BET	TTDEM BET
Surface area		
Range for calculation (relative pressure P/P^0)	0.007-0.305	0.007-0.305
Monolayer volume (ncc/g)	1.716716	1.938747
Specific surface area (m^2/g)	7.469353	8.435395
Correlation factor	0.932341	0.965180
Pore specific volume (cm^3/g)	0	0
Pore specific volume at relative pressure P/P^0	0.9910728	0.9910728
Pore size distribution		
Calculation method	BJH	BJH
Pore size range (diameter)	0.31-1.0	0.31-1.0
Cumulative volume (cm^3/g)	0.06453594	0.06401794
Maximum diameter (nm)	2.827989	2.783253
Average diameter (nm)	700.1907	792.6436

Applied Polymer SCIENCE

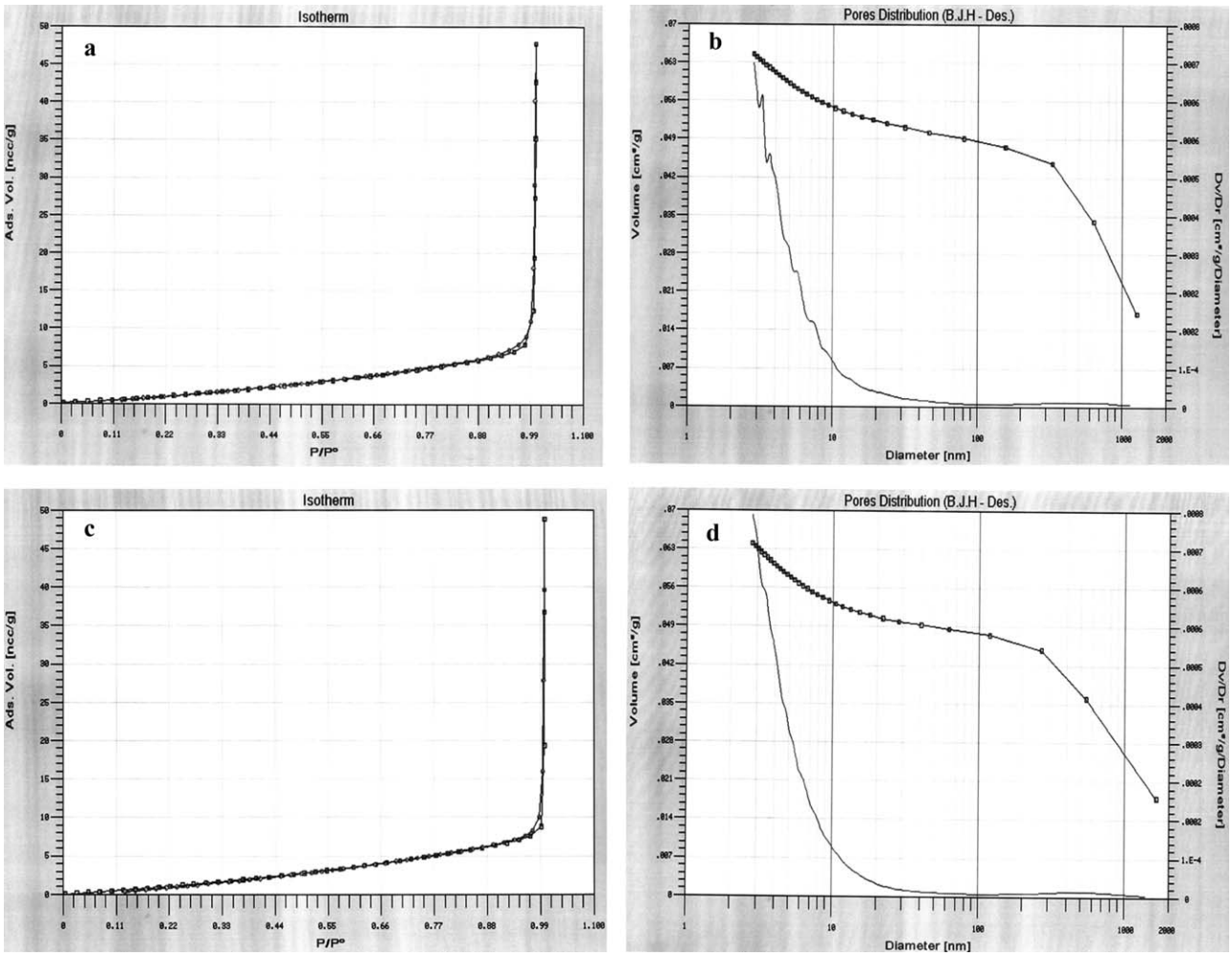

Figure 4. (a) Nitrogen adsorption–desorption isotherm of TTDMM. (b) Pore size distribution for TTDMM. (c) Nitrogen adsorption–desorption isotherms for TTDEM. (d) Pore size distribution for TTDEM.* Ads. Vol = Adsorption volume, D_v = deviation in volume and D_r = deviation in radius

be considered as an asset for drugs. Their larger surface areas and pore sizes could accumulate larger amount of drug as a vehicles in the field of biomedical and biochemical processes. The pore size confirmed that the adsorption-average pore diameters of TTDMM and TTDEM were 792.6436 and 700.1907 nm, as calculated with the BJH method [Table I and Figure 4(b,d)]. The difference in their average pore diameters was 92.4529 nm and was due to the 6-CH_2. The maximum diameter of the pores of TTDMM and TTDEM were 2.827989 and 2.783253 nm, respectively; this proved that the dendrimers had inside pores because of attached malonate esters at the surface [Table I and Figure 4(b,d)]. The higher diameter of the pores for TTDEM, having a —OCH_2CH_3 group at a terminal position, and the lower diameters for TTDMM, with a —O—CH_3 group at the terminal position, implied that their electron-releasing capacity was as follows: —O—CH_3 > OCH_2CH_3.

MD and PDI

The MD and PDI values implied interaction and aggregation behavior of the drug–dendrimer complexes[28] with MD values of 12.00, 11.11, and 1.13 nm for TTDMM, TTDEM, and SB, respectively (Table II). The dendrimers showed higher MD values than SB, with a definite surface area and pore size and a π-conjugated core and dialkyl malonate esters. The MDs were 3.43 and 3.45 nm for SB–TTDMM and SB–TTDEM, respectively. DLS showed a slight decrease in MD with increasing PDI (Table II). MD decreased from 12.00 to 3.43 nm and from 11.11 to 3.45 nm for TTDMM and TTDEM, respectively. PDI increased from 0.0220 to 1.1640 and 0.0218 to 1.1740 upon complexation with SB on effective aggregation. The PDI values

Table II. MD (nm) and PDI Values of TTDMM, TTDEM, SB–TTDMM, and SB–TTDMM

	MD	PDI
TTDMM	12.00	0.0220
TTDEM	11.11	0.0218
SB	1.13	0.0713
SB-TTDMM	3.43	1.1640
SB-TTDEM	3.45	1.1740

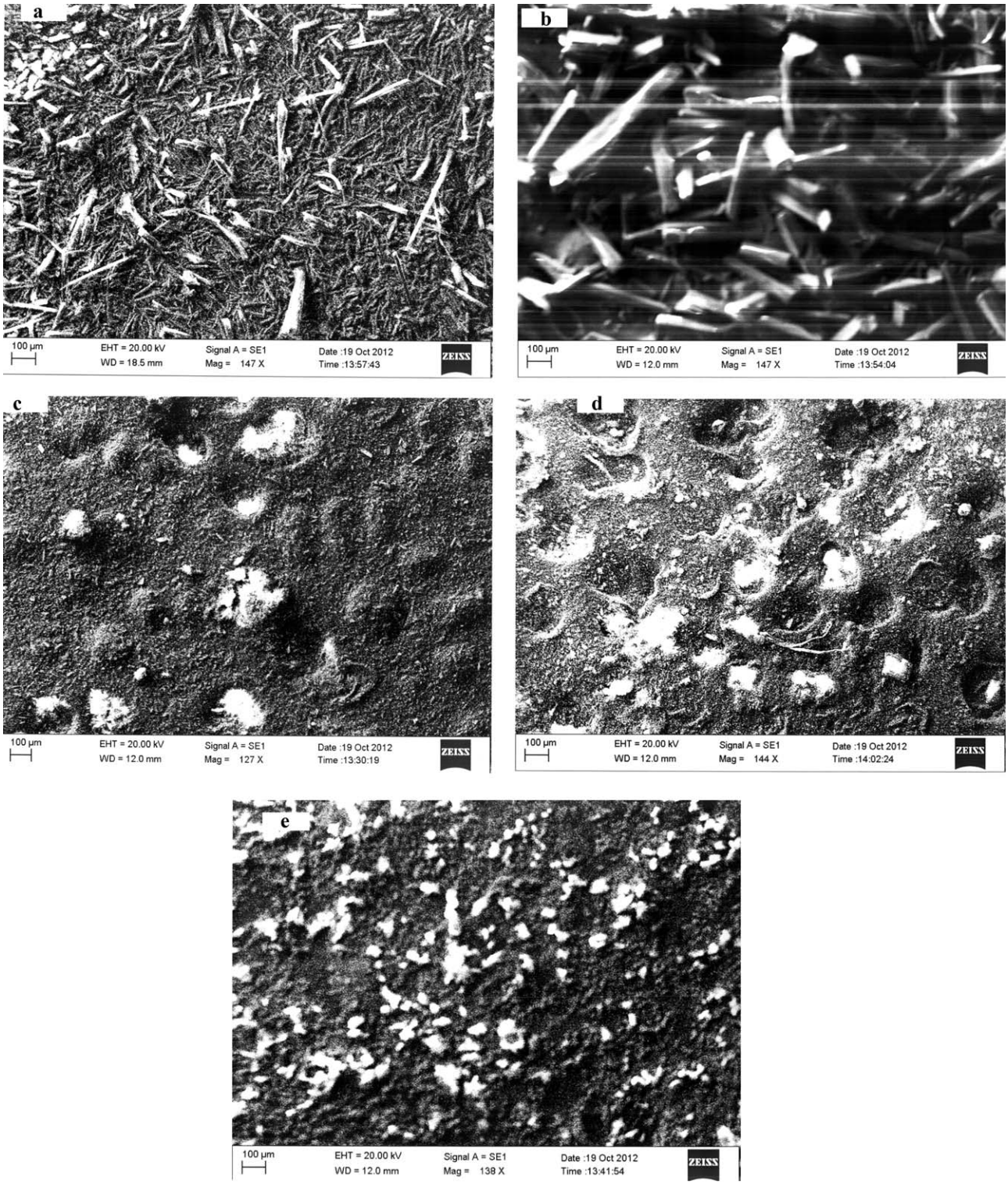

Figure 5. SEM images of (a) TTDMM, (b) TTDEM, (c) SB, (d) SB–TTDMM, and (e) SB–TTDEM.

for TTDMM, TTDEM, and SB were 0.0220, 0.0218, and 0.0718, respectively. PDI for TTDEM was slightly lower than that of TTDMM by 0.002. The PDIs of 1.1740 and 1.1640 were as follows: SB–TTDEM > SB–TTDMM by 0.01, with a higher capacity of TTDEM with increasing alkyl chains compared to TTDMM. The dendrimers with lower MD and higher PDI compared to those of the complexes implied the involvement of interaction and aggregation (Table II). Decreasing the MD from 12.00 to 3.45 nm of the dendrimers and complexes resulted in a significant difference in size (Table II). SB–TTDMM was slightly

Applied Polymer SCIENCE

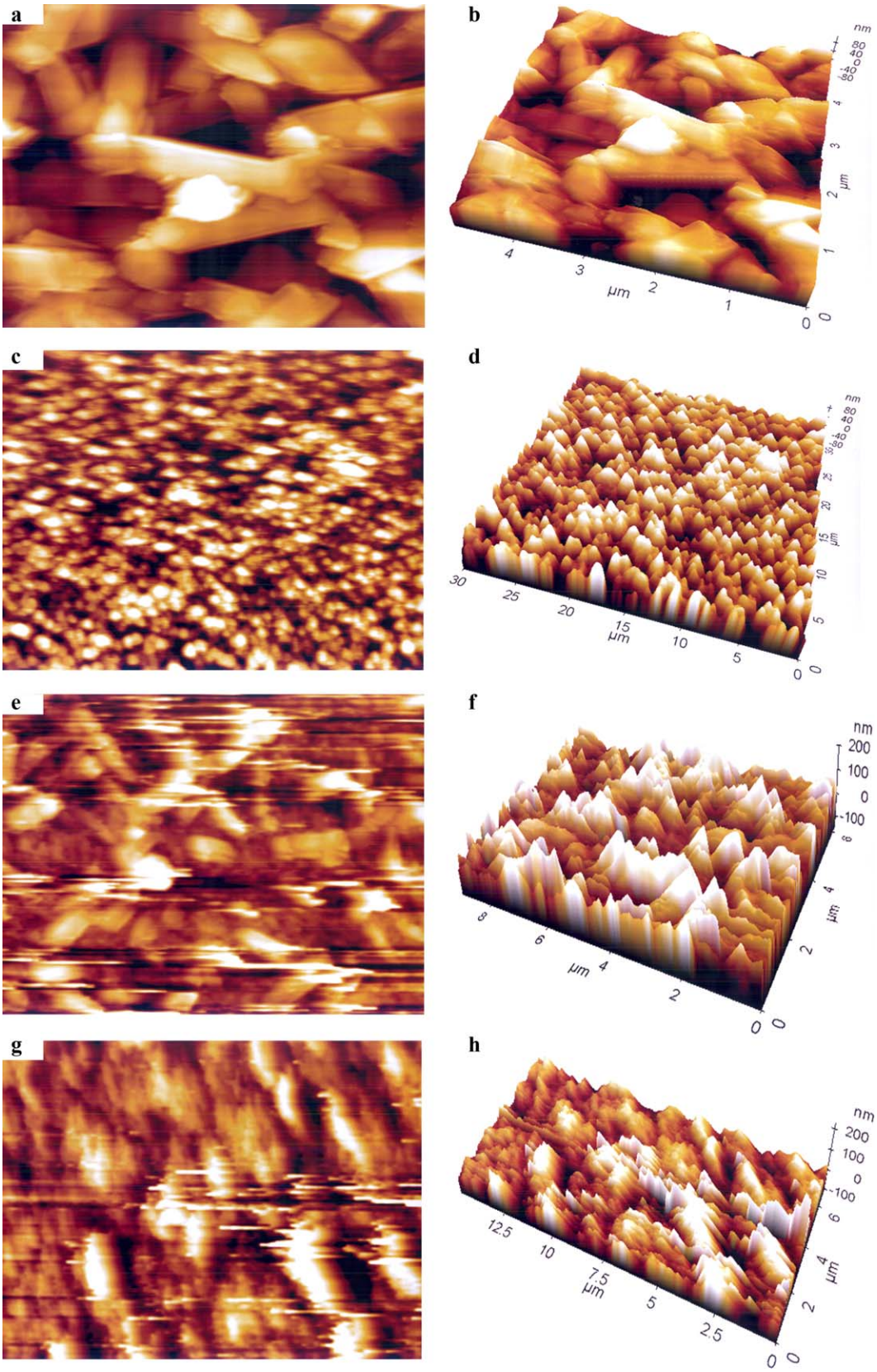

Figure 6. (a) AFM image of TTDMM. (b) AFM 3D image of TTDMM. (c) AFM image of TTDEM. (d) AFM 3D image of TTDEM. (e) AFM image of SB–TTDMM. (f) AFM 3D image of SB–TTDMM. (g) AFM image of SB–TTDEM. (h) AFM 3D image of SB–TTDEM. [Color figure can be viewed in the online issue, which is available at wileyonlinelibrary.com.]

Table III. Statistics of the Selected Region for Topographical Images of TTDMM, TTDEM, SB–TTDMM, and SB–TTDEM

	Min (nm)	Max (nm)	Mean (nm)	R_a (nm)	R_z (nm)	R_{sk}	R_{ku}
TTDMM	−44.672	37.753	0.174	13.960	50.385	0.292	2.853
TTDEM	−33.768	92.603	14.611	18.565	86.556	−0.535	3.577
SB-TTDMM	−71.650	152.879	8.547	32.400	151.824	−0.815	4.042
SB-TTDEM	−41.625	58.274	−0.074	14.095	62.875	−0.544	3.463

Min, minimum height of the region; Max, maximum height of the region; Mean, arithmetic mean height region; R_a, average roughness; R_z, 10-point average roughness of the selected region.

smaller in size than SB–TTDEM. The dendrimers and complexes were not uniform in size, as indicated by the MD and high PDI, this implied the homogeneous distribution of SB without evidence of collapsed particles in the void spaces of TTDMM and TTDEM.

Morphological Study

The SEM micrograph for TTDMM showed an almost equal distribution of molecular geometries with longer and thinner threadlike structures in a form of crystalline shapes. These were branched and distributed with almost equal sizes [Figure 5(a,b)]. As compared to TTDEM, TTDMM showed denser structures, but TTDEM showed a thicker sticklike structure with their equal distribution in two-dimensional surface area. The smaller structures with 100 μm, but in the case of TTDEM, the smaller sized particles were connected to larger sized and larger shaped sparingly particles distributed with a larger surface area. Thus, TTDMM developed a closely packed structure compared to TTDEM. The PDI of TTDMM was 0.0220 with almost equal distribution [Figure 5(a)]. However, SB has showed a globular-type SEM structure with larger sized clusters with almost equal bulk area [Figure 5(c)]. This implied that SB, even with a solid form, had clusters of different geometries that may have been due to many benzene rings with many 5-OH groups whose activities were monitored with their motions. A considerable shift in the distribution of SB with TTDMM is depicted in Figure 5(d); the results imply that the interstices of TTDMM were most effective in holding SB, and the TTDMM acted as cap to hold during the transportation of SB. SB with TTDMM showed intermixing with reverse-mixing trends [Figure 5(d)]. As compared to the SB–TTDMM internal morphology, SB was closely bound with TTDEM because of the —CH_2 activities, where the —CH_2 seemed to be a rider on the structural and functional behavior of the TTDEM as compared to TTDMM. However, with the longer sticklike structure in the case of pure TTDEM, the size with SB was globularized; this implied that the TTTDEM seemed to wrap around the SB to form spherical structures localized in fewer areas compared to TTDEM. This implied that the entropy and IMMFT played a critical role in the optimization of the SB–TTDEM complexes, which may have been operated through friccohesity of the pure TTDEM and the SB–TTDEM complexes. Thus, the critical variations in the internal morphologies of the dendrimers suggested that the SEM images of SB–TTDMM and SB–TTDEM showed SB distributions in their void spaces; this was confirmed by FTIR spectroscopy, DSC, and DLS analysis [Figure 5(d,e)].

Topographical Studies

Topographical images of dendrimers taken with AFM of their thin films coated on glass slides within a 30-μm scan area showed dissimilarity in the images. The topographical observations showed that the dendrimers formed a stable globular and extended monolayer structure because of the alkyl chains at the terminal position as tentacles [Figure 6(a–d)]. The AFM images showed that the SB with TTDMM and TTDEM dendrimers were equally distributed as the dendrimers had a tendency to form a compact and packed structure. The outstanding alignment of the SB structure in TTDMM and TTDEM was shown in their AFM images [Figure 6(e–h)]. The AFM three-dimensional (3D) images showed that the surface topographies of the TTDMM, TTDEM, SB–TTDMM, and SB–TTDEM [Figure 6(b,d,f,h)] were different with individual sets of molecules. The AFM topographical pictures of TTDMM as compared to TTDEM were interlocked with each other, whereas the molecules of TTDEM were similar to the kinds of a flat sheet. Such peculiarities were caused by the —CH_2 activities. The line analysis for the topographical images of TTDMM, TTDEM, SB–TTDMM, and SB–TTDEM minimum surface areas in the selected regions were as follows: −44.672, −33.768, −71.650, and −41.625 nm, respectively (Table III). Also, the maximum surface areas in the selected regions were 37.753, 92.603, 152.879, and 58.274 nm for TTDMM, TTDEM, SB–TTDMM, and SB–TTDEM, respectively. TTDEM had a higher surface area than TTDMM, but after complexation with SB, it showed a reverse trend. The mean height values of the selected region were 0.0174, 14.611, 8.547, and −0.074 nm for TTDMM, TTDEM, SB–TTDMM, and SB–TTDEM, respectively. The

Table IV. Absorbance of the Pure TTDMM and TTDEM and the SB Concentration in PBS with 10% DMSO

	TTDMM	TTDEM			
Concentration		λ_{max} (nm)	SB		
(μM)	240 nm	240 nm	245 nm	285 nm	330 nm
25	0.508	0.154	0.242	0.224	0.518
50	0.870	0.251	0.465	0.454	1.074
75	1.182	0.425	0.682	0.678	1.606
100	1.208	0.568	0.890	0.918	1.987
125	1.236	0.695	1.107	1.170	2.187

Applied Polymer SCIENCE

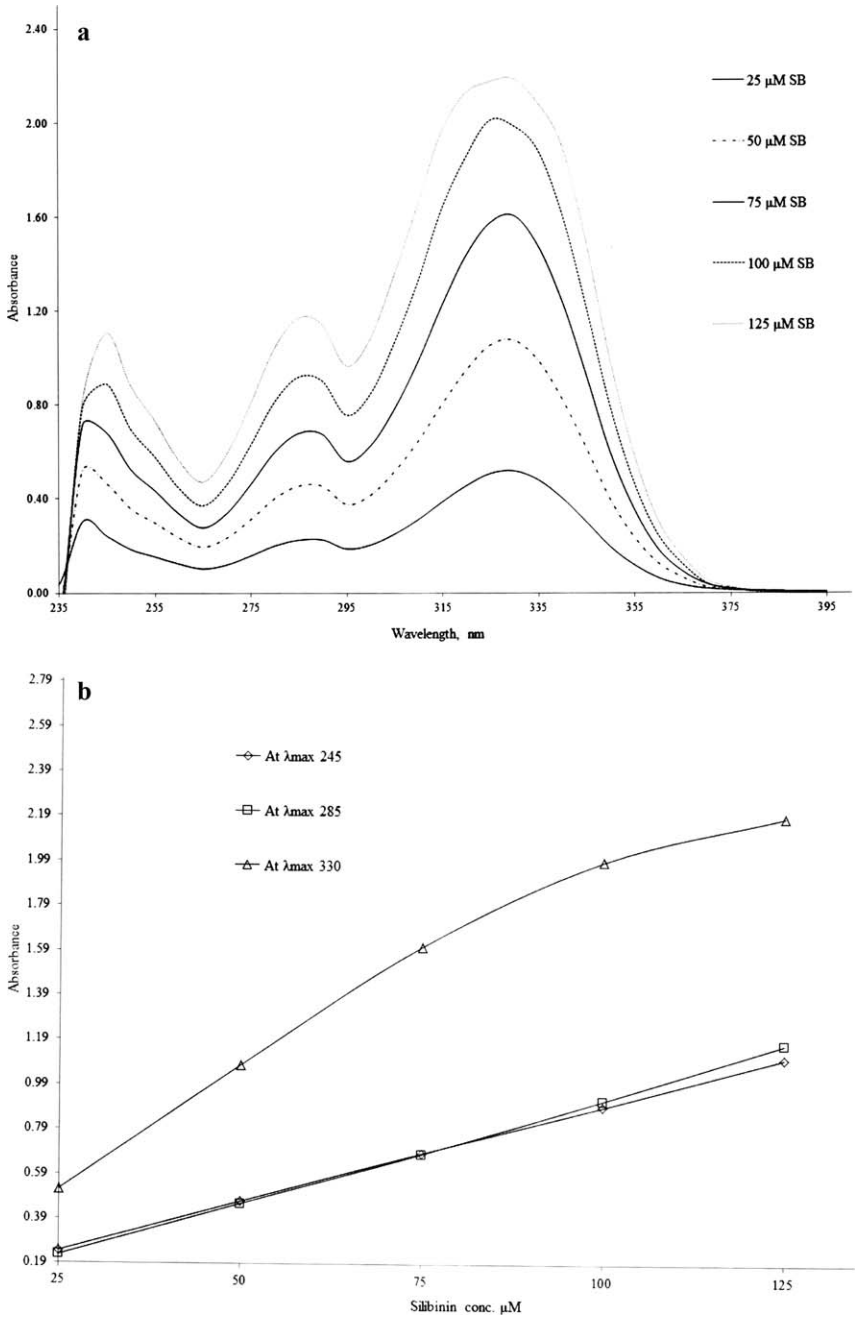

Figure 7. (a) UV–vis absorbance spectra of SB. (b) Standard absorbance calibration curve of SB at λ_{max} values of 245, 285, and 330 nm.

average roughness area and 10-point average roughness in selected regions (Table III) for topographical images of dendrimers and complexes were compared and implied a role of interstices. The higher average roughness of TTDEM compared to that of TTDMM was seen as due an additional —CH_2 with TTDEM, and the same trend was found with their complexes. The skewness (R_{sk}) values are given in Table III for selected regions of topographical images have implied R_{sk} of the dendrimers and complexes (Table III). The kurtosis (R_{ku}) values of a line are also shown in Table III; they implied the spikiness of the dendrimers and complexes. We found a higher value of SB–TTDMM compared to that of SB–TTDEM. Similarly, the 3D images of TTDMM were similar to a rectangular shape with wider gaps in between, whereas the 3D images of TTDEM had a kind of regular pattern with comparatively higher thicknesses in the z direction because of the impact of the —CH_2 on topographies. However, the pattern of the 3D images of SB depicted shown in Figure 6(f) implied a comparatively higher thickness with higher width; this could be attributed to the presence of several benzene rings and —OH functional groups in its structure. Such a structure could also be favorable for being bound by dendrimers.

Table V. Absorbance for the SB Released at 0–10 h at λ_{max} Values of 245, 285, and 330 nm from the SB–TTDMM and SB–TTDEM Complexes

	SB-TTDMM			SB-TTDEM		
Time (h)	245	285	330	245	285	330
0	0.938	0.123	0.144	0.057	0.016	0.019
1	1.364	0.709	1.419	0.638	0.595	1.399
2	1.466	1.017	1.654	0.831	0.768	1.712
3	1.463	1.055	1.638	0.569	0.561	1.268
4	1.500	1.123	1.678	0.856	0.824	1.777
5	1.466	0.971	1.635	0.831	0.782	1.693
6	1.553	1.060	1.708	1.025	0.978	1.928
7	1.662	1.249	1.830	0.892	0.836	1.750
8	1.623	1.083	1.790	0.899	0.841	1.772
9	1.770	1.398	1.917	0.924	0.844	1.767
10	1.757	1.428	1.914	1.003	0.89	1.824

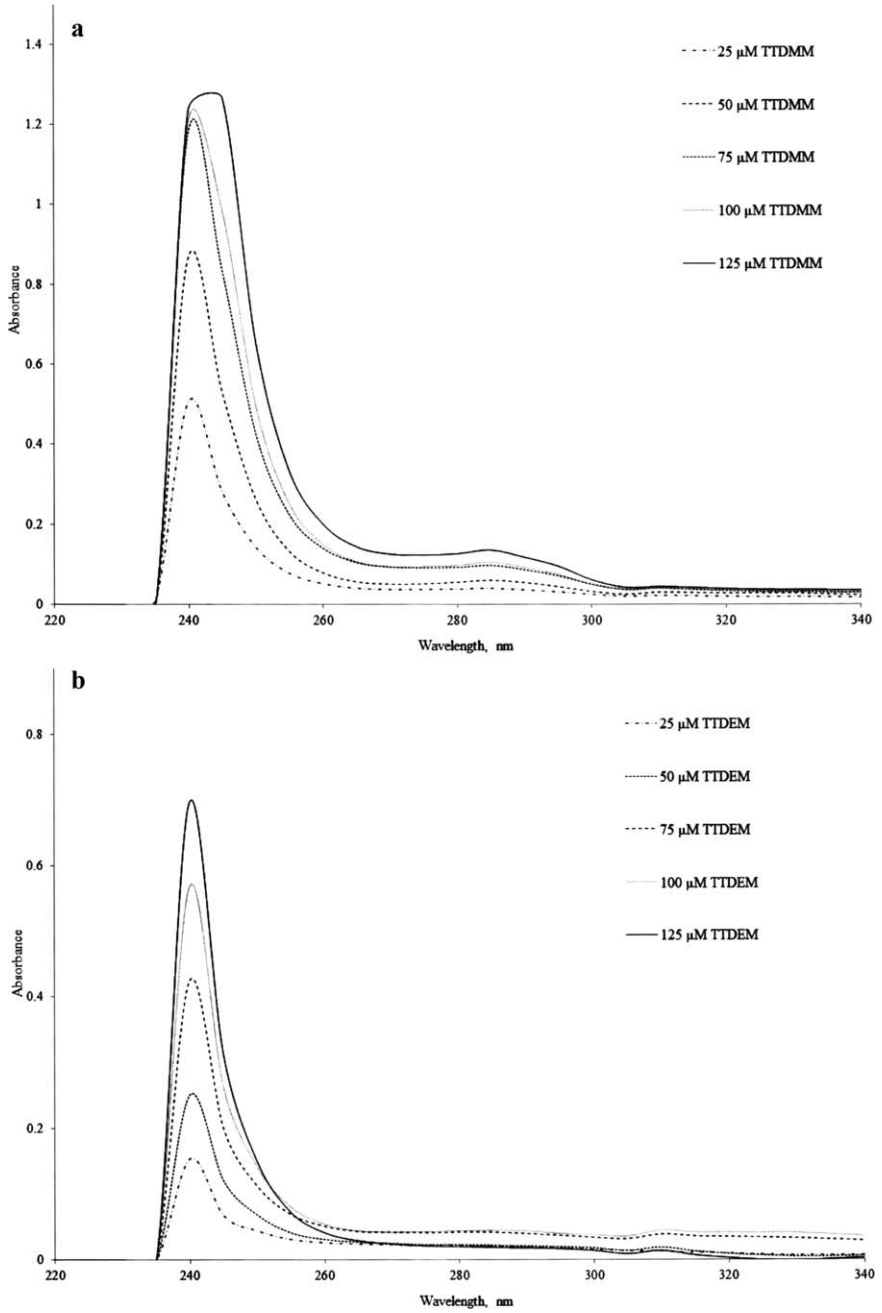

Figure 8. UV–vis absorbance spectra of (a) TTDMM and (b) TTDEM.

Applied Polymer SCIENCE

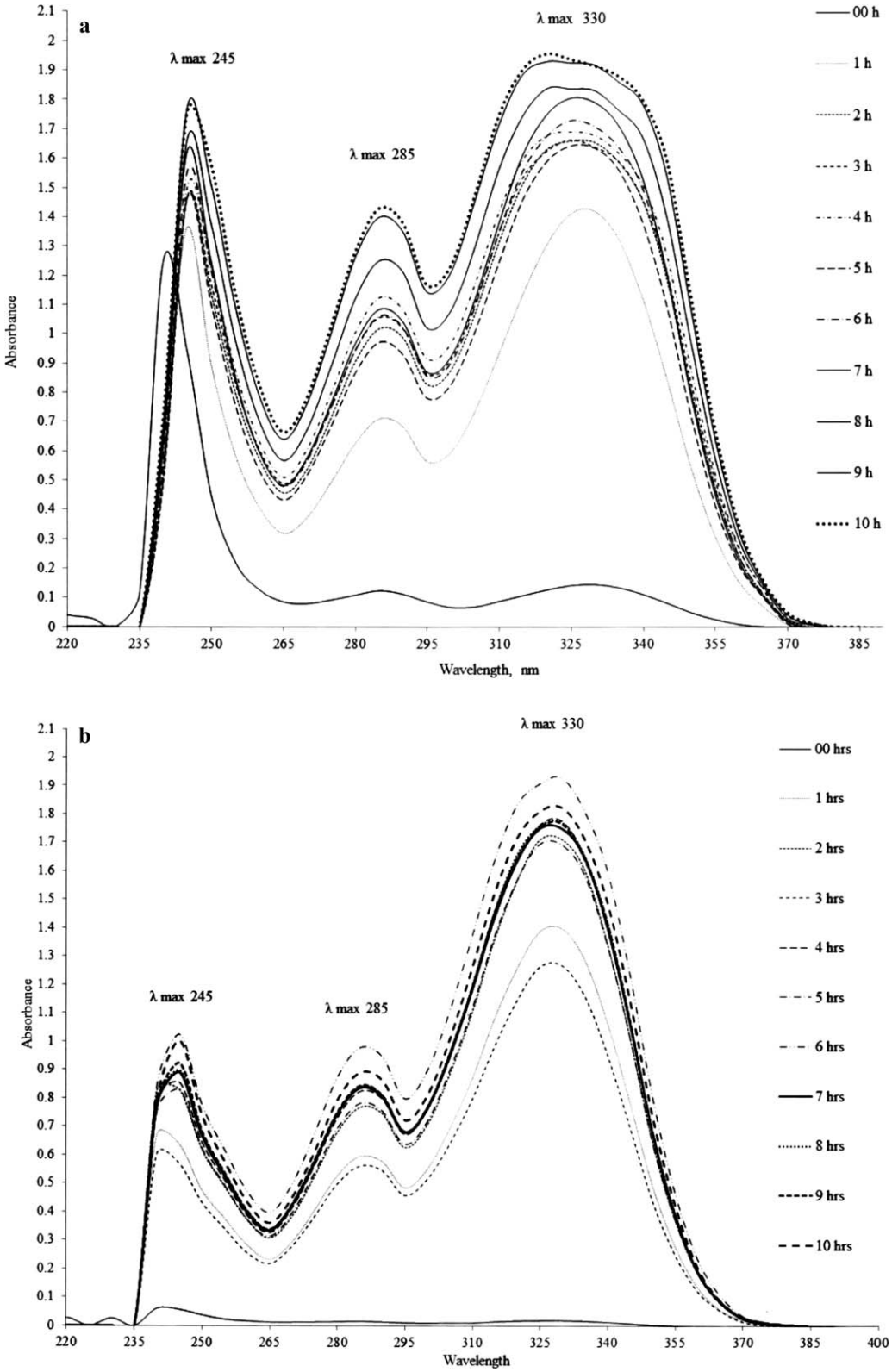

Figure 9. UV–vis absorbance spectra of (a) SB–TTDMM and (b) SB–TTDEM.

In Vitro Release Study

The UV absorbance values increased with increasing concentrations of TTDMM, TTDEM, and SB in PD (Table IV). Thus, the observations obtained through the SEM and AFM images implied that the SB was structurally stabilized in both dendrimers because it was trapped in the interstices of the

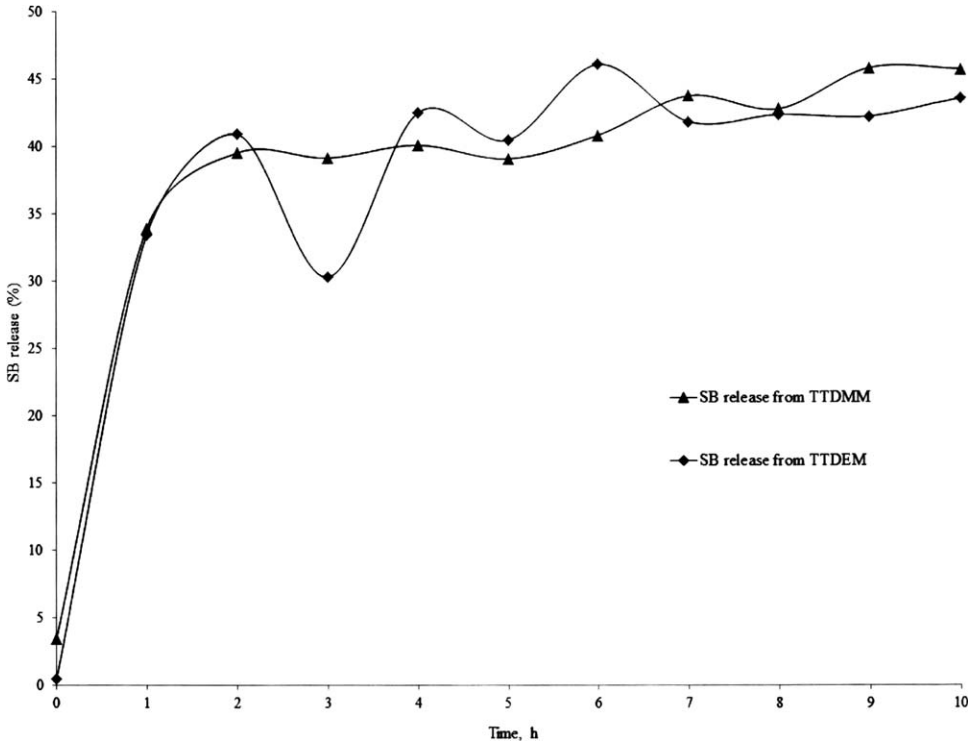

Figure 10. SB release (%) from TTDMM and TTDEM.

dendrimers with the development of interaction through the hydrogen bond (HB) between them. The SB with 5-OH groups and >CO groups of dialkyl malonate esters in interstices were accountable for the HB interactions along with oscillations of the tentacles of the dendrimers. The 25, 50, 75, 100, and 125 μM concentrations in PD and SB showed absorbance bands at λ_{max} of 245, 285, and 330 nm. The SB moles with PD developed an internal pressure with a higher SB binding with PD, and no micelle formation took place [Table IV and Figure 7(a)]. Linear calibration curves derived from the absorbance versus SB concentration plotted at λ_{max} values of 245, 285, and 330 nm [Figure 7(b)] showed that at high λ_{max} values, the absorbance varied with concentrations of 25, 50, 75, 100, and 125 μM, but at λ_{max} values of 245 and 285 nm, a slightly lower difference between the SB absorbance at the same concentration took place. The absorbance was higher at a λ_{max} value of 330 nm for the SB compared to those at λ_{max} values of 245 and 285 nm. The SB standard calibration curve was determined in PD with correlation coefficients (R^2's) of 0.9999, 0.9995, and 0.9700 at λ_{max} values of 245, 285, and 330 nm, respectively, for 25–125 μM SB [Table V and Figure 7(b)] with the higher energy and binding capacity of the SB with PD. For similar compositions of TTDMM and TTDEM in PD, λ_{max} was at 240 nm, and there were variations in their absorbance from 0.0508 to 1.236 for TTDMM and 0.154 to 0.695 for TTDEM [Table IV and Figure 8(a,b)]. The absorbances of TTDMM that were greater than those of TTDEM implied more activities of alkyl chains with PD. A pattern of their distribution in PD remained similar to continuous clustering or micropatches, with more clustering attained at a λ_{max} value of 240 nm. However, with the 25–125 μM dendrimers in PD showed variation in their absorbance [Figure 8(a,b)]. SB–TTDMM and SB–TTDEM with PD were analyzed for the release of SB from the complex at 0–10 h. λ_{max} appeared at 245, 285, and 330 nm in 1–10 h and at λ_{max} = 240 nm, but it disappeared with both of the dendrimers (Table V). However, the same was present in their standard composition with PD [Table IV and Figures 8(a,b) and 9(a,b)]. Figure 9(a,b) shows that the same pattern of absorbance and λ_{max} of SB were found in PD [Figure 7(a)] and were reproduced with a slight variation in their absorbance because of the binding capacity of dendrimers. The absorbance with SB slightly increased from 1 to 10 h; this implied SB release from the complexes (Figure 10). This was very surprising, in that λ_{max} with SB in PD showed a sharp peak but λ_{max} with the dendrimers showed a broad peak [Figures 7(a) and 9(a,b)]. Furthermore, the peaks at a λ_{max} value of 330 nm were much broader compared to those of SB with PD; this may have been due to activities of the tiers. The broadness of the peaks proved that SB was trapped in a structure of tiers, and the SB distribution area in the dendrimers was larger than that of SB in PD. The dendrimers implied a homogeneous distribution of SB in larger amounts. Surprisingly the broadness was higher for TTDMM as SB was held by methyl groups instead of ethyl groups. After about 6 h, about 40 and 45% SB were observed to be released from TTDMM and TTDEM, respectively (Figure 10). A higher, approximately 4% rate of SB was released from TTDEM s compared TTDMM at 1–10 h. The higher amount of SB released from TTDEM compared to that of TTDMM implied that the SB was held by TTDMM instead of TTDEM. The dimethyl and DEMEs

were attached at terminal positions of TTDMM and TTDEM, respectively, and they were responsible for holding SB by HB interactions. The additional σ bond of diethyl malonate in TTDEM weakened the HB interaction compared to dimethyl malonate in TTDMM in the PD medium. The TTDMM-driven distribution of SB in a similar medium seemed to be most effective compared to TTDEM.

CONCLUSIONS

TTDMM and TTDEM with wider surface areas and pore sizes seemed significant for adsorption applications with higher activities with an increase in alkyl chains. Variations observed in DSC, FTIR spectroscopy, NMR, surface area, and pore size distribution in TTDEM compared to TTDMM implied a larger contribution of $-CH_2$. The higher binding capacities of TTDMM and TTDEM for the encapsulation of SB were retrieved by FTIR spectroscopy, DSC, SEM, AFM, and DLS for targeting and intracellular drug-delivery capabilities. The dendrimers with mechanical branches were referred to as tentacles, which assisted in the trapping of targeted SB for successful drug impacts on diseases like cancer.

ACKNOWLEDGMENTS

The authors are thankful to Central University of Gujarat, Gandhinagar, for infrastructural support, and University Grants Commission, Government of India, New Delhi, India, for financial support (Gov. F. No.38-51/2009 SR).

REFERENCES

1. Buhleier, E.; Wehner, W.; Vogtle, F. *Synthesis* **1978**, *2*, 155.
2. Tomalia, D. A.; Baker, H.; Dewald, J.; Hall, M.; Kallos, G.; Martin, S.; Ryder, J.; Smith, P. *Polym. J.* **1985**, *17*, 117.
3. Frechet, J. M. *J. Science* **1994**, *263*, 1710.
4. Vogtle, F.; Getermann, S.; Hesse, R.; Schwierz, H.; Windisch, B. *Prog. Polym. Sci.* **2000**, *25*, 987.
5. Frechet, J. M.; Hawker, C. J.; Wooley, K. L. *Pure Appl. Chem. A* **1994**, *31*, 1627.
6. Singh, M.; Yadav, D.; Yadav, R. K. *J. Polym. Sci.* **2008**, *110*, 2601.
7. Medina, S. H.; El-Sayed, M. E. *Chem. Rev.* **2009**, *109*, 3141.
8. Tomalia, D. A.; Baker, H.; Dewald, J.; Hall, M.; Kallos, G.; Martin, S.; Roeck, J.; Ryder, J.; Smith, P. *Macromolecules* **1986**, *19*, 2466.
9. Tomalia, D. A.; Drust, H. D. *Top. Curr. Chem.* **1993**, *165*, 193.
10. Singh, M. *Bull. Chem. Soc. Ethiop.* **2011**, *25*, 119.
11. Singh, M.; Gupta, S. *Synth. Commun.* **2008**, *38*, 2898.
12. Singh, M.; Pandey, M. *Phys. Chem. Liq.* **2008**, *46*, 119.
13. Singh, M.; Kumar, V. *Int. J. Thermodyn.* **2007**, *10*, 121.
14. Newkome, G. R.; Yao, Z. Q.; Baker, G. R.; Gupta, V. K.; Russo, P. S.; Saunders, M. J. *J. Am. Chem. Soc.* **1986**, *108*, 849.
15. Nalylor, A. M.; Goddard, W. A., III; Kiefer, G. E.; Tomalia, D. A. *J. Am. Chem. Soc.* **1989**, *111*, 2339.
16. Jansen, J. F.; De Brabandader-van den Berg, G. A.; Meijer, E. W. *Science* **1994**, *266*, 1226.
17. Hawker, C. J.; Wooley, K. L.; Frechet, J. M. *J. Chem. Soc. Perkin Trans.* **1993**, *1*, 1287.
18. Malik, N.; Evagorou, E. G.; Duncan, R. *Anti-Cancer Drugs* **1999**, *10*, 767.
19. Zhuo, R. X.; Du, B.; Lu, Z. R. *J. Controlled Release* **1999**, *57*, 249.
20. Brunauer, S.; Emmett, P. H.; Teller, E. *J. Am. Chem. Soc.* **1938**, *60*, 309.
21. Barrett, E. P.; Joyner, L. G.; Halenda, P. P. *J. Am. Chem. Soc.* **1951**, *73*, 373.
22. Hu, Y.; Jiang, X.; Ding, Y.; Zhang, L.; Yang, C.; Zhang, J.; Chen, J.; Yang, Y. *Biomaterials* **2003**, *24*, 2395.
23. Kalkotwar, R. S.; Kasture, A. V.; Pattan, S. R.; Dengale, S. S.; Dighe, N. S. *Der Pharma Chem.* **2010**, *2*, 127.
24. Park, E. K.; Lee, S. B.; Y. Lee, M. *Biomaterials* **2005**, *26*, 1053.
25. Ling, Y.; Huang, Y. *IFMBE Proc.* **2008**, *19*, 514.
26. Potts, J. R.; Dreyer, D. R.; Bielawski, C. W.; Ruoff, R. S. *Polym.* **2011**, *52*, 5.
27. Singh, M. *J. Appl. Polym. Sci.* **2004**, *92*, 3437.
28. Wang, C.; Wyn-Jones, E.; Tam, K. C. *Colloids Surf. A* **2010**, *364*, 49.